ORGANOMETALLICS

pubs.acs.org/Organometallics Article

Mechanistic Insights into C−H Borylation of Arenes with Organoiridium Catalysts Embedded in a Microporous Metal−Organic Framework

Zoha H. Syed, Zhihengyu Chen, Karam B. Idrees, Timothy A. Goetjen, Evan C. Wegener, Xuan Zhang, Karena W. Chapman, David M. Kaphan,* Massimiliano Delferro,* and Omar K. Farha*

Cite This: https://dx.doi.org/10.1021/acs.organomet.9b00874 Read Online

ACCESS | Metrics & More | Article Recommendations | Supporting Information

ABSTRACT: Organometallic iridium catalysts can be used in conjunction with bispinacolatodiboron (B_2Pin_2) to effect the borylation of a variety of substrates such as arenes, alkanes, heteroarenes, and oxygenates. Recently, efforts have also focused on integrating these catalysts into porous supports, such as metal−organic frameworks (MOFs). While the mechanism of homogeneous borylation systems has been thoroughly investigated experimentally and computationally, analogous studies in MOF-supported iridium catalysts have not been conducted. Herein, we report the mechanistic investigation of a phenanthroline-iridium catalyst immobilized in the organic linker of Universitetet i Oslo (UiO)-67 ($Zr_6O_4(OH)_4(BPDC)_4(PhenDC)_2$, BPDC = biphenyl-4,4′-dicarboxylate, PhenDC = 1,10-phenanthroline-4,4′-dicarboxylate). By using benzene as a model substrate, variable time normalization analysis (VTNA) of the kinetic data suggested a rate law consistent with zero-order in B_2Pin_2, and first-order in arene. A primary kinetic isotope effect (KIE) in the time course of benzene-d_6 borylation also provided complementary information about the role of the arene in the rate-determining step of the reaction. Characterization by techniques such as X-ray absorption spectroscopy (XAS) confirmed the presence of Ir(III), while pair distribution function (PDF) analysis suggested structures containing an Ir−Cl bond, further substantiated by X-ray photoelectron spectroscopy (XPS). Analysis of postcatalysis materials by inductively coupled plasma−optical emission spectroscopy (ICP-OES) revealed low boron accumulation, which may indicate an absence of boron in the resting state of the catalyst. Finally, in comparing borylation of benzene and toluene, a slight selectivity for benzene is observed, which is similar to the analogous homogeneous reaction, indicating the influence of substrate sterics on reactivity.

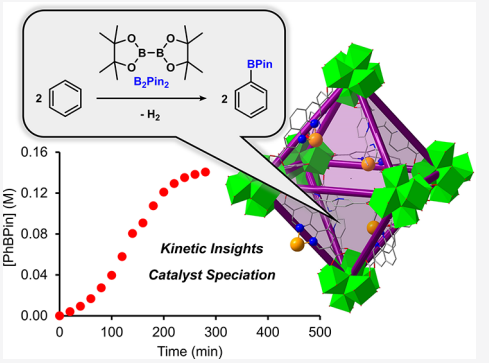

INTRODUCTION

The functionalization of C−H bonds in abundant, natural feedstocks remains a pervasive challenge in the petrochemical and pharmaceutical industries.[1,2] For further derivatization, installation of reactive moieties is often required for subsequent transformation to commodity chemicals.[1,2] An example of such is the catalytic incorporation of C−B bonds to hydrocarbons, forming products such as boronic esters or boronates, that can serve as useful synthons for a variety of reactions such as cross-coupling, conjugate addition, and oxidative amination.[3−5]

In particular, borylation methodologies catalyzed by iridium-based catalysts have shown promise.[3−5] Smith and co-workers first reported the borylation of aryl substrates using a Cp*Ir(PMe_3)(H)(BPin) (17 mol %, Cp* = pentamethylcyclopentadienyl, BPin = pinacolboryl) catalyst (Figure 1A).[6−8] Monoborylated benzene (phenylboronic acid pinacol ester, PhBPin) was formed in 53% yield after 120 h at 150 °C using pinacolborane (HBPin) as the borylating agent. Smith and co-workers expanded their investigation to phosphine-ligated iridium catalysts as well, which showed enhanced activity in comparison to their previously reported Cp*Ir systems.[3,8] Hartwig, Miyaura, Ishiyama, and co-workers later reported the borylation of arenes using combinations of dimeric iridium(I) precursors, such as $[Ir(COD)X]_2$ (where COD = 1,5-cyclooctadiene and X = Cl or OMe), and bidentate nitrogen donor ligands such as 2,2′-bipyridine (bpy) or 4,4′-ditertbutyl-2,2′-bipyridine (dtbpy) (Figure 1B).[9,10] In the presence of bispinacolatodiboron (B_2Pin_2) or HBPin, arenes and heteroarenes[2−5,9−18] could be used to form arylboronate esters with turnover numbers as high as 24 000, ranging from room temperature to 80 °C.[3,9,19]

Since the report of these seminal examples, investigation has continued into optimization of borylation systems through

Special Issue: Organometallic Chemistry at Various Length Scales

Received: December 27, 2019

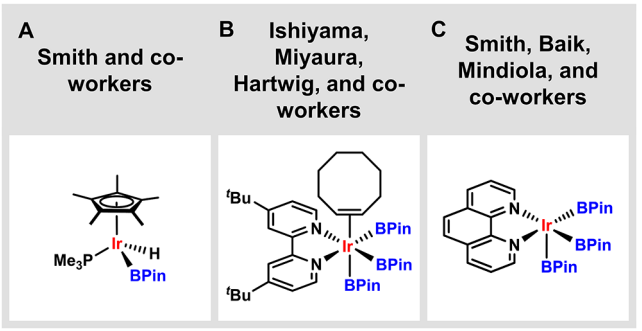

Figure 1. Homogeneous, organoiridium catalysts for borylation. (A) Smith and co-workers, $Cp^*Ir(PMe_3)(H)(BPin)$ for borylation of arenes. (B) Ishiyama, Miyaura, Hartwig, and co-workers $(dtbpy)Ir(BPin)_3(COE)$, active for borylation of arenes upon dissociation of COE. (C) Smith, Baik, Mindiola, and co-workers, proposed active catalyst for methane borylation, studied computationally.

ligand modification and expansion to other classes of substrates, beyond arenes.[2−4,11,20−30] In particular, efforts have expanded to functionalizing light alkanes such as methane, which is particularly difficult due to the chemical inertness of the C−H bonds. Sanford and co-workers contemporaneously with Smith, Baik, and Mindiola and co-workers reported the borylation of methane using iridium catalysts in combination with ligands such as 1,10-phenanthroline derivatives (Figure 1C).[26,27] At 150 °C and high pressures of methane in the presence of B_2Pin_2, a mixture of monoborylated and diborylated products could be obtained.[26,27]

To improve the chemoselectivity and efficiency of borylation reactions, efforts have begun and continued toward the immobilization of efficient molecular catalysts into porous supports.[31−40] In such a scenario, the molecular, architectural features of the support can impart a shape selective effect, thus using size exclusion to improve selectivity for one product over another. Moreover, grafting of an organometallic fragment onto a heterogeneous support may generate single site catalysts with enhanced activity, likely due to decreased catalyst deactivation. One class of inorganometallic materials that can be used for this application is metal−organic frameworks (MOFs). Featuring inorganic nodes and organic linkers, they are known for their high porosity, crystallinity, and diverse structural features. Moreover, MOF-supported catalysts offer an opportunity to study structure-activity relationships in a single-site heterogeneous catalyst system.[40] Indeed, the successful incorporation of organoiridium-based borylation catalysts has occurred in MOFs for borylation of substrates such as arenes and methane.[34,35,37,39−41] In particular, we recently reported the incorporation of 1,10-phenanthroline into a UiO-67-type framework, which generated a mixed linker MOF comprised of 4,4′-biphenyldicarboxylate (BPDC) and 1,10-phenanthroline-4,4′-dicarboxylate (PhenDC) (UiO-67-mix) (Figure 2).[40] Upon metalation with $[Ir(COD)Cl]_2$ and subsequent oxidation in ambient atmosphere, a single-site Ir(III) catalyst was generated (Figure 2, vide infra) that proved to be competent for the chemoselective monoborylation of methane, likely due to tailored pore size and aperture.[40]

As catalytic competency for borylation has been widely demonstrated with organometallic iridium catalysts, interest has grown in the mechanism of these processes. In the molecular, *N,N*-ligand/Ir(I) systems, Hartwig and others, through extensive kinetic study and structural characterization,[4,5,7,11,14,19,20,22,25,27,42−47] proposed the catalytic cycle depicted in Scheme 1. A five coordinate Ir(III)trisboryl active

Scheme 1. Proposed Ir(III)/Ir(V) Catalytic Cycle for Homogeneous Borylation of Hydrocarbons with an *N,N*-Bidentate Ligand Scaffold

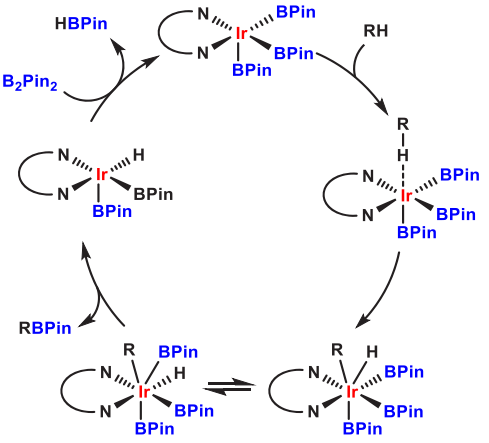

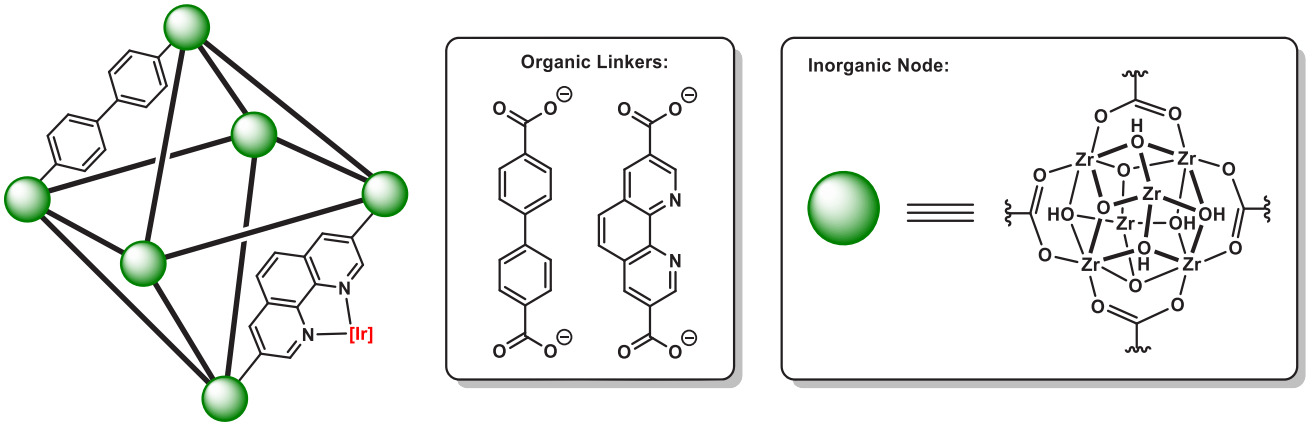

Figure 2. Structure of mixed-linker MOF UiO-67-mix, comprised of biphenyl-4,4′-dicarboxylate (BPDC) and 1,10-phenanthroline-4,4′-dicarboxylate (PhenDC) organic linkers bound to Zr-based cluster nodes. Octahedral pore is shown for clarity, and ligands other than phenanthroline have been omitted from the inner coordination sphere of the iridium center for clarity.

https://dx.doi.org/10.1021/acs.organomet.9b00874
Organometallics XXXX, XXX, XXX−XXX

intermediate, which is generated from dissociation of COE (COE = cyclooctene) from the metal center, can activate the arene substrate through oxidative addition or σ-bond metathesis, with the former being more likely (Scheme 1). This seven-coordinate Ir(V) adduct is then proposed to undergo isomerization, followed by reductive elimination of the PhBPin product (Scheme 1). The Ir(III)trisboryl is then regenerated following reaction with B_2Pin_2 (Scheme 1). This has also been supported computationally[23,25,27,45,47] and is hypothesized to be the mechanistic pathway with other organometallic iridium complexes as well.[27,34]

Computational investigation of the borylation mechanism in an Ir catalyst immobilized in a MOF has also been carried out. Gagliardi and co-workers studied the mechanism of methane borylation with UiO-67-mix-Ir to gain insight into the origin of the chemoselectivity that was observed.[48] It was found that the Ir center inside the MOF had similar reactivity to the homogeneous analogues, proceeding through an iridium-trisboryl intermediate. The selectivity for monoborylated methane originated from a larger barrier of diffusion (24.7 kcal/mol) for the diborylated product, which is 14.2 kcal/mol higher than that for monoborylated methane. In addition, the rate-determining step was found to be isomerization of the seven coordinate Ir(V) rather than C−H bond cleavage via oxidative addition as in the homogeneous reaction.[48]

The kinetic and mechanistic implications of MOF immobilization of iridium borylation catalysts, however, have not been thoroughly investigated, experimentally. Herein, we examine the mechanism of borylation with UiO-67-mix-Ir catalysts. Using benzene as a model substrate, for ease of handling and higher activity, kinetic data was collected, and catalyst speciation was studied. Vapor-phase sorption studies were used to gain insight into affinity of the Ir catalyst for benzene. Time course profiles revealed an induction period in benzene borylation, which is effected by the concentration and nature of arene that is present. A comparison of benzene and toluene borylation indicated similar substrate selectivity to the corresponding homogeneous reaction. Characterization of UiO-67-mix-Ir postcatalysis also showed low boron content present in the material, which may indicate little boron accumulation in the catalyst in its resting state, representing a departure from previously reported homogeneous systems.

RESULTS AND DISCUSSION

Synthesis and Characterization of UiO-67-mix and UiO-67-mix-Ir Materials. UiO-67-mix (**1**) was synthesized according to our reported sample preparation[40] (for spectroscopic characterization confirming catalyst integrity, see the Supporting Information, pages S15−41[40] for further discussion and characterization). The MOF was then metalated with iridium via solvothermal deposition in MOFs (SIM) at room temperature under inert atmosphere, using a modification of the previously reported preparation (see the Supporting Information for further discussion).[40] Upon addition of $[Ir(COD)Cl]_2$ and anhydrous tetrahydrofuran (THF), the off-white MOF turned green (Figure S1), consistent with chelation of the Ir(I) precursor by the 1,10-phenanthroline linker.[49] Upon shaking overnight, to facilitate mass transport, under inert argon atmosphere, the suspension changed from green to blue (Figure S1), likely due to the coordination of Cl^- to the Ir center, as observed by Colacot and co-workers with homogeneous (phen)Ir complexes[49] (vide infra), forming UiO-67-mix-Ir(I) (**2**, see the Supporting Information for characterization).[49] Exposure of **2** to ambient atmosphere results in a color change from blue to orange, generating the Ir(III) material, UiO-67-mix-Ir(III) (**3**), which had previously shown competency for chemoselective methane borylation.[40] Following washing and soaks in acetone overnight to remove residual water and activation under high vacuum at 150 °C overnight, the N_2 isotherm for **3** showed a decrease in surface area from 2430 m^2/g to 1550 m^2/g, with a corresponding decrease in quantity of N_2 adsorbed (Figure S4 and S8), though the pore width distribution remained relatively unchanged, centered at ∼1.0 nm. Powder X-ray diffraction (PXRD) patterns confirmed crystallinity and phase purity was maintained after postsynthetic metalation and thermal activation (Figure S5 and S9). Inductively coupled plasma-optical emission spectroscopy (ICP-OES) confirmed Ir loading onto the MOF—approximately two Ir atoms per Zr_6 node were present (∼13 wt % Ir, Table S2), which corresponded to the approximately two PhenDC linkers per Zr_6 node.

While structural elucidation by single crystal X-ray diffractometry of **2** and **3** was precluded due to the disordered nature of the mixed-linker MOF, X-ray pair distribution function (PDF)/difference envelope density (DED) analyses (dPDF, Figure 3A), X-ray absorption spectroscopy (XAS), and DRIFTS were used to probe the ligand environment around the as-prepared iridium materials.

High resolution X-ray powder diffraction patterns were collected for the native MOF **1**, and the Ir(I) and Ir(III) metalated MOFs, **2** and **3** respectively, after which PDF/DED analyses were conducted. In all three samples, crystallinity was maintained (Figure S3). DED analysis revealed electron density centered around the linkers of samples **2** and **3**, consistent with Ir chelated by the phenanthroline linkers and was localized to the octahedral pore of **1** as opposed to the tetrahedral pore based on PDF/DED analysis, on average (Figure S40−S43). PDF analysis confirmed the integrity of the UiO-67 framework in all samples, though slight distortion of the Zr_6 node was observed after postsynthetic modification of the native MOF.

A comparison between **3** and authentic samples of $[Ir(COD)Cl]_2$ and (phen)Ir(COD)(Cl)[49](a molecular analogue to the proposed structure of **2**, where Cl^- is in the inner coordination sphere) by X-ray absorption near edge structure (XANES) indicates changes to the local coordination of iridium upon metalation and air exposure. The increased white line intensity suggests the presence of Ir(III) in **3** (Figure S19) and the EXAFS are consistent with the first coordination sphere consisting of light-scattering atoms (i.e., C, N, or O) (fitting results in Table S8), both consistent with previously reported results of **3**.[40]

Upon conducting differential pair distribution function (dPDF) analysis, with **1** as a reference, local information regarding the guest iridium and its interactions with the frameworks in **2** and **3** could be obtained. Three atom−atom distances in particular were observed in various magnitudes, centered at ∼2.1, ∼2.4, and ∼3.0 Å (Figure 3A). On the basis of previous structural characterization of organometallic phenanthroline-iridium complexes, the distance at 2.1 Å could be assigned to bonds such as Ir−N, Ir−O, or Ir−C (consistent with EXAFS) and 3.0 Å to longer range interactions such as that between Ir and aromatic carbon atoms on the phenanthroline backbone (Figure 3A). A distance at 2.4 Å is consistent with the presence of Ir−Cl in

https://dx.doi.org/10.1021/acs.organomet.9b00874
Organometallics XXXX, XXX, XXX−XXX

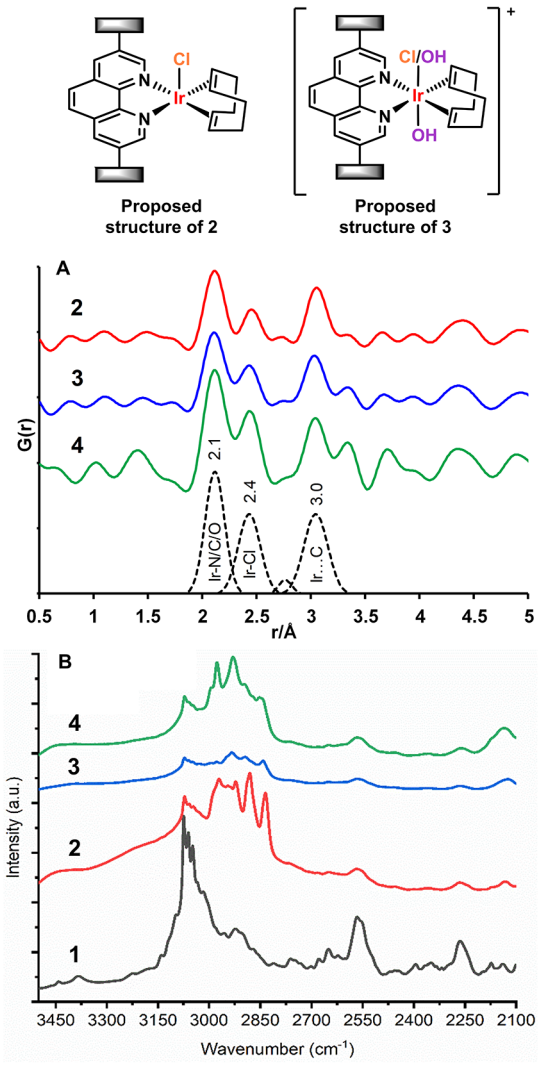

Figure 3. Characterization of **1**, **2**, **3**, and **4** by X-ray PDF and DRIFTS for investigation of catalyst structure. (A) dPDF patterns showing the presence of Ir N/C/O bonds and an Ir−Cl bond, which could be present in **2** and **3**. (B) DRIFTS spectra of Ir-metalated samples **2**−**4** in comparison to native MOF **1** (not commonly scaled) showing the growth of aliphatic C−H stretches likely associated with COD ligand. A proposed structure for **2** may include an inner sphere chloride bound to Ir with COD, generating an 18 electron Ir(I) adduct inside the MOF. Upon exposure to ambient atmosphere to form **3**, oxidation/hydrolysis can occur, leading to coordination of hydroxyl groups. The presence of COD by DRIFTS may suggest a cationic Ir(III) 18 electron complex being formed inside the MOF as a mixture of species with or without inner sphere chloride. A chloride ion in the outer coordination sphere for structure **3** has been omitted for clarity.

samples **2** and **3** (Figure 3A), which is not observed in EXAFS fittings, likely due to the overlap of multiple scattering paths in the first coordination sphere. The presence of Ir−Cl in **2** and **3** was further confirmed by X-ray photoelectron spectroscopy (XPS), where peaks in the Cl 2p region were observed at binding energies consistent with metal-chloride bonds being present in the samples (Figure S25−S33).[50]

Diffuse reflectance infrared Fourier transform spectroscopy (DRIFTS) was also used for structural elucidation of **2** and **3** (Figure 3B). Upon metalating native MOF **1** with $[Ir(COD)Cl]_2$, the retention of aromatic stretches associated with the MOF organic linkers along with new aliphatic C−H stretches around 2850 cm^{-1} are observed, consistent with coordination of COD to the iridium center of **2**. After oxidation to Ir(III), **3** retains aliphatic C−H stretches, suggesting COD is still bound to the metal center (Figure 3B). Thus, through a combination of the aforementioned techniques, precatalyst structures can be proposed for **2** and **3**. The Ir(I) analogue **2** likely contains an inner sphere chloride bound to the Ir center as well as COD, forming a five coordinate 18 electron complex analogous to homogeneous phenanthroline-iridium species formed in THF using $[Ir(COD)Cl]_2$ as the metalating agent with 1,10-phenanthroline.[49] Upon oxidation to Ir(III), retention of COD ligand on the Ir center may be consistent with formation of a cationic six coordinate 18 electron complex such as that in Figure 3, in which there is coordination of X-type ligands such as hydroxide or chloride, likely resulting in a mixture of species inside the MOF.

Benzene Affinity in UiO-67-mix-Ir via Vapor Sorption and Catalytic Benzene Borylation. To demonstrate the viability of benzene as a borylation substrate and explore its potential interactions with the Ir center, vapor-phase sorption data were collected for native MOF **1** and UiO-67-mix-Ir(III) **3**. The adsorption isotherms for benzene were collected for **1** and **3** at 338 K to probe interaction of the vapor source with the material similar to reaction conditions and determine propensity for adsorption (Figure 4). The adsorption is at ∼7 mmol/g for **1** and ∼3 mmol/g for **3** at about 20 mmHg partial pressure of benzene—the disparity between uptake likely due to the decrease in pore volume upon metalation of **1** with Ir (Figure 4A). A steeper uptake of benzene is observed at low pressure (<3 mmHg) for **3** in comparison to **1**, which is indicative of a relatively higher affinity of **3** with benzene in comparison to the native MOF (Figure 4B).

To investigate the reversibility of adsorption, a second cycle of benzene sorption was conducted, following reactivation of the samples at 338 K under vacuum. Similar adsorption isotherms are obtained, with steeper uptake observed once again at low pressure (<3 mmHg) for **3** in comparison to **1** (Figure S46−S47). The steep uptake may suggest a strong but reversible interaction between benzene and the metalated MOF.

Having observed this affinity for benzene by **3**, catalytic studies of benzene borylation with B_2Pin_2 as the limiting reagent were subsequently pursued (Scheme 2). In the borylation of benzene, 2 equiv of PhBPin can be formed per mole of B_2Pin_2 in a one-pot reaction, liberating H_2. The first equivalent of PhBPin can be formed from borylation of benzene with B_2Pin_2, forming product and HBPin (Figure S48). The second equivalent of PhBPin can form through concomitant borylation with in situ generated HBPin, which can also be consumed over the course of the reaction, forming dihydrogen (H_2). This manifests as low HBPin accumulation over the course of the reaction. Indeed, in using HBPin as a borylating agent in place of B_2Pin_2, PhBPin could be formed (for further discussion, see the Supporting Information, page S44).

To minimize variation, all reaction kinetics experiments were conducted using the same batch of catalyst (see the Supporting Information, page S9 and S48, for discussion of batch to batch variation in catalyst performance). In a stirred reaction with benzene (1.93 M) and B_2Pin_2 (0.073 M) in the presence of **3** (40 mg, 12 mol % catalyst loading, catalyst loading = mmol Ir/mmol B_2Pin_2 as a percentage) and cyclohexane solvent,

https://dx.doi.org/10.1021/acs.organomet.9b00874
Organometallics XXXX, XXX, XXX−XXX

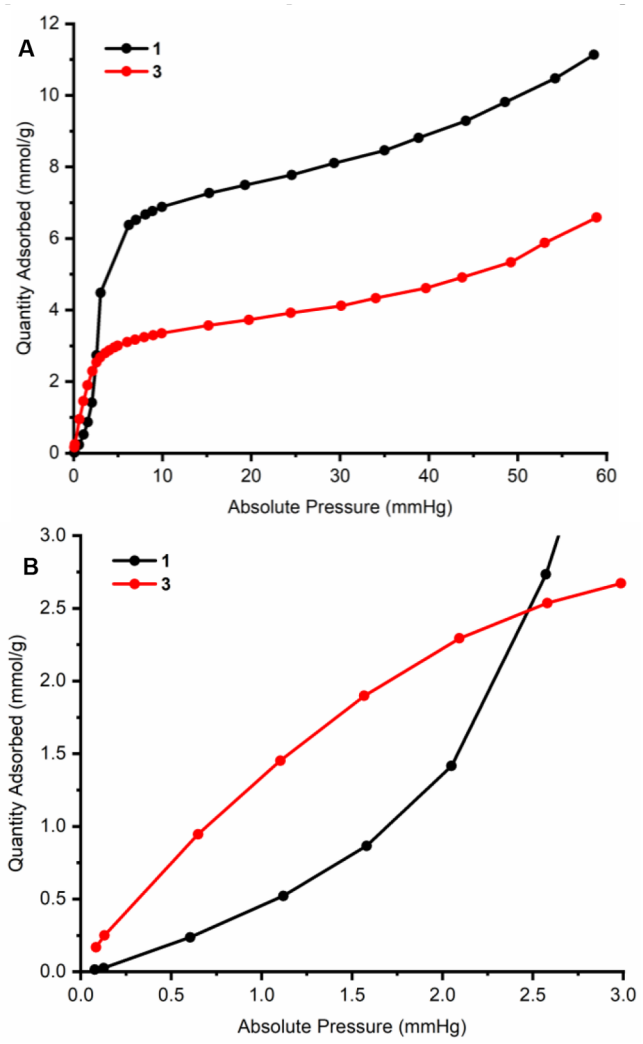

Figure 4. Benzene vapor sorption of **1** and **3** at 338 K with (A) showing overall uptake and (B) showing low pressure region (<3 mmHg) where a sharp uptake of benzene is observed with **3** in comparison to **1**. See the Supporting Information for discussion of conditions.

Scheme 2. Benzene Borylation with 3 to Form PhBPin

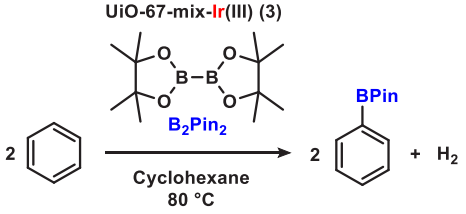

borylation of benzene to PhBPin (selective for monoborylation) was observed in quantitative conversion of B_2Pin_2 over the course of 280 min at 80 °C (~16 turnovers, turnover = mmol PhBPin/mmol Ir) (Figure 5). In analyzing the mass balance of the reaction (see the Supporting Information, pages S48−51), fluctuations from 100% are likely due to accumulation of HBPin and/or physisorption of reactants and products within the porous material. A hot filtration test confirmed the heterogeneity of the reaction and ICP-OES analysis of the postcatalysis material showed retention of Ir loading. In addition, control borylation experiments in the absence of catalyst showed no benzene borylation (see the Supporting Information, page S45−S46). Through monitoring of the reaction over time by gas chromatography-flame ionization detection (GC-FID), in the presence of hexadecane as an internal standard, an induction period was revealed in the first ~60 min of reaction after which it reached quantitative conversion of starting material (Figure 5A,B). Upon decreasing the concentration of benzene while holding concentration of B_2Pin_2 constant, an apparent elongation of the induction period was observed, with little PhBPin observed after 280 min using the lowest concentration of 0.22 M benzene (Figure 5C,D). When comparing two concentrations of B_2Pin_2 (Figure 5E,F), a slight inhibitory effect that elongates the induction period at higher concentration is observed compared to lower concentration as reaction with 0.037 M B_2Pin_2 appears to reach quantitative conversion faster than that which is using 0.146 M. If activation of the arene is requisite for induction, increased concentration of B_2Pin_2 relative to benzene may lead to competition of pore occupation between the two substrates, which could result in elongation of the induction period. Alternatively, the arene could be involved in turnover after induction, at which point pore blockage by B_2Pin_2 can occur. In either mechanistic scenario, B_2Pin_2 may have an inhibitory effect.

To further interrogate kinetic dependence on concentration in the region most influenced by induction, variable time normalization analysis (VTNA) was performed (Figure 6).[51−53] This analysis was first conducted on a series of experiments designed to assess rate dependence on concentration of catalyst. Upon variation of the catalyst loading from 20 mg to 40 mg to 80 mg, VTNA revealed a change in catalyst order gradually—the reaction remained first-order in catalyst in the first ~50 min (Figure 6A,B) after which deviation from first-order behavior began to occur. This suggests the development of mass transport limitations over time during the reaction, which is believed to occur through adhesion of catalyst to the walls of the reaction vessel, leading to uneven mixing which generally coincided with the onset of mass transfer effects. Bearing this in mind, visual kinetic analysis was performed on profiles with variable concentrations of benzene and B_2Pin_2, with deviations to partial order rate dependence likely taking place due to mass transport. VTNA of a plot of varying concentration of benzene (Figure 6C) began showing overlap when fit to a first-order rate dependence on the concentration of benzene, though optimal overlap is observed when fit to a 0.75 order rate dependence (Figure 6D). As VTNA is designed to extract information on rate dependence of the reaction, it is likely borylation occurs first-order in arene after induction; however, an alternative interpretation of these data is that the generation of the active catalyst is first order in arene and the subsequent catalytic turnover is zero-order in arene. The latter interpretation cannot be discounted based on these data. In contrast, visual fit was achieved in varying B_2Pin_2 concentration plots near zero-order (Figure 6E), with optimal fit occurring in fits of −0.1 order (Figure 6F), precluding a positive rate dependence on B_2Pin_2. As with benzene, deviation to a partial order in B_2Pin_2 is also observed over time, which is likely due to mass transport. A slight inhibitory effect of B_2Pin_2 is also observed in this reaction, notably at earlier time points in the region of induction, and thus a negative order in B_2Pin_2 is in accord with this observation. The borylation reaction is likely zero-order in B_2Pin_2 after induction. The observation of this zero rate dependence, however, precludes it from being

https://dx.doi.org/10.1021/acs.organomet.9b00874
Organometallics XXXX, XXX, XXX−XXX

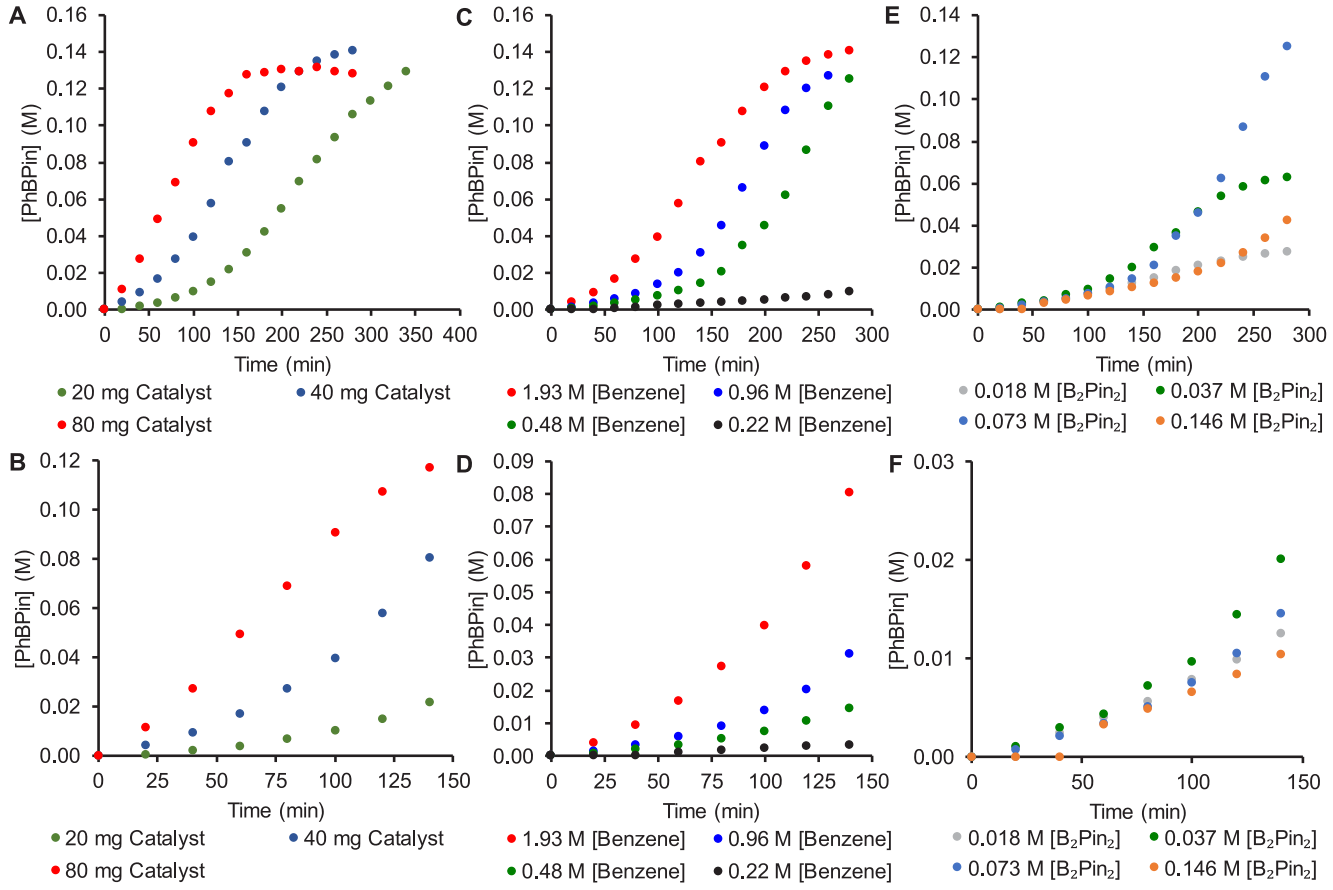

Figure 5. Benzene borylation monitored over time by GC-FID at 80 °C stirring at 1000 rpm in cyclohexane solvent, (A) variation of catalyst loading monitored over time with 0.073 M [B_2Pin_2] and 1.93 M [benzene], (B) early reaction time region of catalyst loading rate dependence, (C) variation of benzene concentration monitored over time with 0.073 M [B_2Pin_2] and 40 mg catalyst, (D) early reaction time region of benzene concentration rate dependence, (E) variation of B_2Pin_2 concentration monitored over time with 0.48 M [benzene] and 40 mg catalyst, (F) early reaction time region of B_2Pin_2 concentration rate dependence.

involved in the chemical transformation at the Ir center to generate the active catalyst during the induction period. Thus, consistent with these observations is a rate law that is first-order in iridium and arene and close to zero-order with a slight inhibitory effect in B_2Pin_2. This rate law bears resemblance to the previously reported homogeneous rate law for arene borylation,[19] though the observed kinetic effects may also be associated with generation of the active catalyst. Nonetheless, the aforementioned kinetic data implicates the arene in the rate-determining step of the reaction.

To further explore the role of arene, the borylation reaction was conducted with benzene-d_6 to probe for isotope effects (Scheme 3A,B). In monitoring the reaction over time by GC-FID (Figure 7), the reaction progresses with a significantly decreased initial rate. Comparison of the two kinetic profiles shows a deviation in rates, consistent with a primary kinetic isotope effect (KIE) in benzene (Figure 7). This may be indicative of rate-limiting C−H bond cleavage during this period. This is either in formation of the active catalyst or the reaction following activation. The presence of this isotope effect agrees with both of these mechanistic scenarios. This isotope effect is a departure from previously reported conclusions in which isomerization of an Ir(V) intermediate was implicated in the rate-limiting step.[48]

The borylation of toluene was next investigated in order to study the effect of arene identity on the reaction (Scheme 4A,B, H_2 omitted from reaction scheme for clarity). In replacing benzene with toluene for borylation (Scheme 4A), a similar total concentration of borylated toluene is produced (Table 1, entries 1 and 2) with quantitative conversion of B_2Pin_2. Borylation of toluene at the *para*- and *meta*- positions is observed in relatively equimolar amounts, with only trace amounts of the *ortho*- product observed. This is consistent with the regioselectivity observed in Hartwig's homogeneous Ir borylation systems, which is driven by sterics of the substrate.[9] To determine if there is selectivity present for one substrate over another, a competition experiment of benzene and toluene borylation was conducted (Scheme 4B). Borylation of both substrates was observed with a 3:1 selectivity for benzene borylation over toluene borylation, with similar regioselectivity of toluene borylation observed to a reaction in the absence of benzene (Table 1, entry 3). This selectivity for benzene borylation over toluene borylation is similar to that which is observed in the analogous homogeneous reaction (Table 1, entry 4). We hypothesize this selectivity for benzene borylation over toluene borylation may be dictated by the sterics of the substrate, an effect that is intrinsic to the phenanthroline-iridium borylation system.

To determine if size selectivity was operant within this system, *t*-butylbenzene was next used in a borylation reaction instead of benzene and B_2Pin_2 conversion was analyzed at the conclusion of the reaction (see the Supporting Information,

https://dx.doi.org/10.1021/acs.organomet.9b00874
Organometallics XXXX, XXX, XXX−XXX

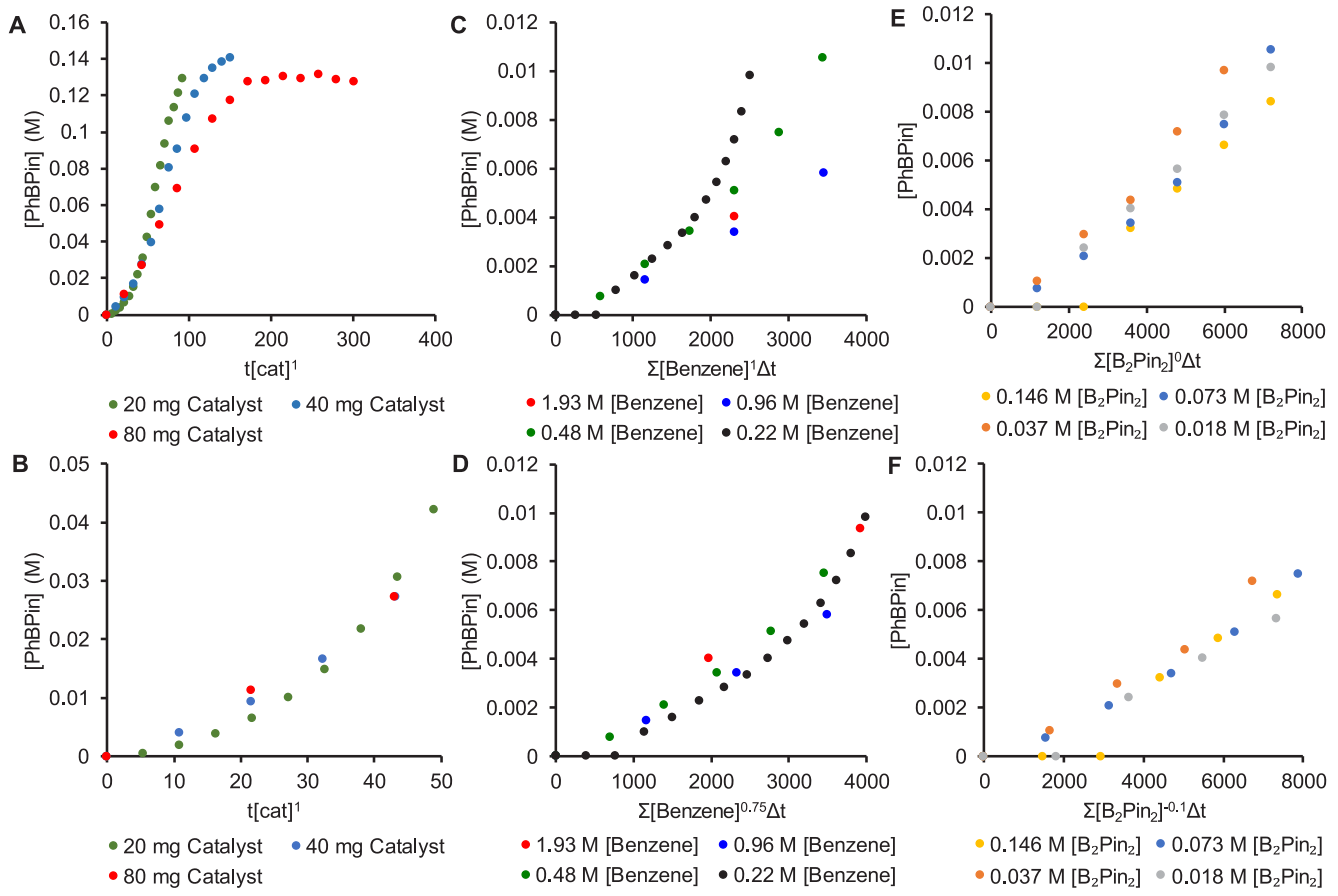

Figure 6. VTNA of benzene borylation monitored over time by GC-FID at 80 °C stirring at 1000 rpm in cyclohexane solvent, (A) VTNA of catalyst loading rate dependence, (B) early reaction time region of catalyst loading rate dependence VTNA, (C) VTNA of benzene concentration rate dependence, (D) early reaction time region of benzene concentration rate dependence VTNA, (E) VTNA of B_2Pin_2 concentration rate dependence, (F) early reaction time region of B_2Pin_2 concentration rate dependence VTNA.

Scheme 3. Benzene vs Benzene-d_6 Borylation with 3 to Determine Kinetic Isotope Effect from Two Parallel Reactions

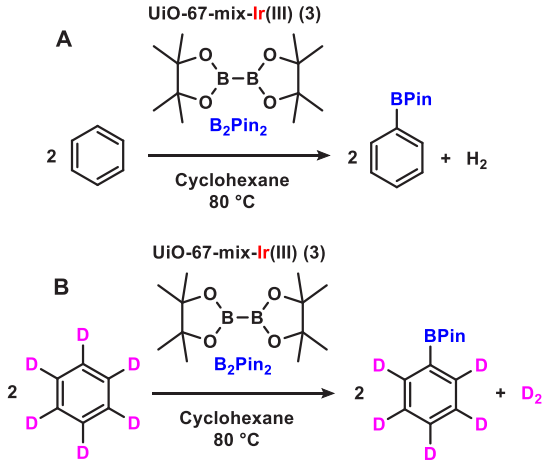

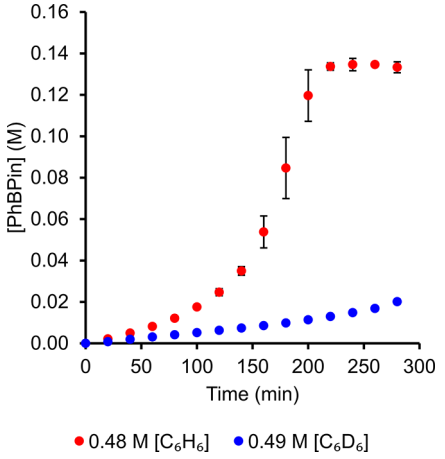

Figure 7. Investigation of the isotopic dependence of benzene borylation by comparing time profiles of benzene borylation to benzene-d_6 borylation monitored over time by GC-FID at 80 °C stirring at 1000 rpm in cyclohexane solvent. Error bars represent the standard deviation of the reactions; for low values, the error bars may be behind the graphical marker, thus they are also included in the Supporting Information.

page S67, for further discussion). A change in B_2Pin_2 concentration was not observed in the reaction of *t*-butylbenzene after 3 h in comparison to that which is observed with benzene (Table S22), in addition to no borylated products being detected. This suggests substrates larger than toluene are sterically constrained from accessing the active sites located in the pores of the MOF, leading to a low turnover frequency and/or delayed catalyst activation.

Characterization of Postcatalysis Materials and Mechanistic Hypotheses. To gain insight into the potential

https://dx.doi.org/10.1021/acs.organomet.9b00874
Organometallics XXXX, XXX, XXX−XXX

Scheme 4. Benzene vs Toluene Borylation with 3 to Determine Substrate Selectivity

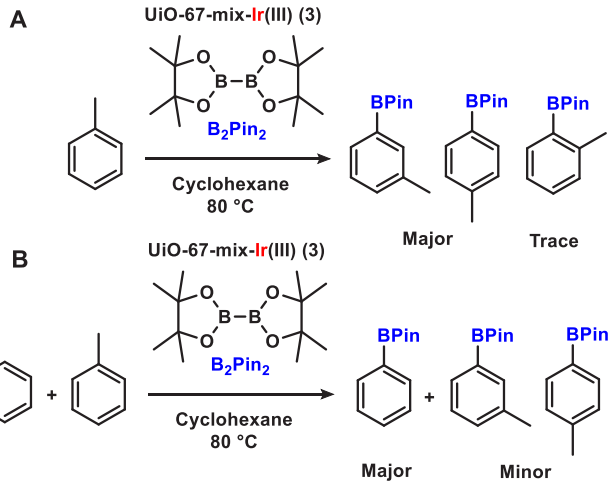

resting state of **3**, the post-catalysis material (**4**) was characterized after isolation from the reaction mixture through centrifugation/decantation and washes with pentane without exposure to air (see the Supporting Information for further discussion). Analysis of the supernatant of the borylation reaction to generate **4** by GC-FID confirmed it had reached completion. Analysis of **4** by N_2 sorption, following activation under high vacuum at 25 °C, showed a BET surface area of 1050 m^2/g with a slight decrease in the pore volume. PXRD patterns showed crystallinity was retained in the catalyst post-borylation and phase purity was also maintained.

ICP-OES analysis was used to assess quantity of boron in the post-catalysis material. This would give insight into the presence of potential Ir-boryl species in postcatalysis materials, as what was observed in analogous homogeneous reactions. Following acid digestion of **3** in a quartz reaction vessel, to assess the "base-line" boron levels in as-prepared samples, a ratio of ∼0.17 B/Ir was obtained, which may occur from presence of adventitious boron from borosilicate vessels and/or tools used prior to digestion (see the Supporting Information, page S26 for further discussion). Analysis of **4** by ICP-OES after subtracting baseline boron quantity results in a ratio of ∼0.42 B/Ir, showing an increase in boron from baseline levels, but an overall lack of accumulation of boron in the post-catalysis sample. If a uniform amount of Ir-boryl was formed in this material, as what was observed in the molecular case, a ratio greater than 1 for B/Ir would be expected, with a theoretical ratio of 3 B/Ir for Ir-trisboryl. The native MOF is capable of encapsulating one iridium-trisboryl species in the octahedral pore as computationally modeled by Gagliardi and co-workers.[48] As there are approximately three to four organometallic iridium species in the octahedral pore of the MOF, having uniform iridium-trisboryl structures for all of them would likely create too much steric congestion for borylation to take place within the pores of the MOF. Thus, this suggests a lack of a boryl species in the catalyst resting state, lack of uniformity in active site structures for the catalyst, or a combination thereof. The residual levels of boron may also be due to physisorbed borylated compounds that were not removed after washing, which could preclude a boron-containing species being operant in the catalysis.

To further probe post-catalysis structure, the material was analyzed by XAS as well as PDF/DED. Negligible changes were observed in the EXAFS and XANES regions of the post-catalysis material in comparison to **3**. DED analysis of **4** was also similar to **3**, demonstrating a lack of movement of Ir within the sample (Figure S44). PDF analysis revealed slight Zr node distortion within the sample; however, no significant changes were observed to the UiO-67 framework. Following dPDF analysis, the same peaks observed in **3** were also observed in **4**, though in different magnitudes (Figure 3A). Interestingly, an Ir−Cl bond was still present in **4**, (Figure 3A) which was substantiated by the presence of Cl in the Cl 2p region probed by XPS. Analysis of the post-catalysis material by DRIFTS (Figure 3B) yielded a similar spectrum to **3**, with aromatic and aliphatic C−H stretches retained in the sample.

In order to probe the induction period further, a post-borylation sample was resubjected to reaction conditions and monitored over time (see the Supporting Information, page S68, for further discussion). A similar induction period was observed, followed by catalytic turnover with a greater maximum instantaneous rate than that observed with the pristine material. Similarly, when a quantity of HBPin was added to a borylation reaction with B_2Pin_2 at the start of the reaction, the reaction rate was observed to be marginally faster however an induction period still remained (Figure S49).

This may be consistent with a mechanistic scenario in which the induction period can stem from a combination of chemical conversion to generate the catalytically active species and/or the buildup of sufficient reactant concentration within the pores of the MOF in order for the reaction to proceed. Following the induction period, two mechanistic hypotheses emerge. Likely the resting state of the catalyst remains Ir(III) as evidenced by similar XANES spectra of **3** and **4**. A low B/Ir ratio may suggest active site nonuniformity, in which case an Ir-trisboryl could be generated in low concentrations and proceed through the Ir(III)/Ir(V) cycle that has been proposed by others.[4] Alternatively, this may imply that a species such as Ir-monoboryl is being generated that can also access the Ir(III)/Ir(V) cycle, proceeding through the same elementary reaction steps as the Ir-trisboryl complex. Further investigation will be required to interrogate this.

Table 1. Borylation of Benzene and Toluene in Cyclohexane Solvent Reveals Differences in Substrate Selectivity[a]

entry	[benzene] (M)	[toluene] (M)	[PhBpin] (M)	[*p*-TolBpin] (M)	[*m*-TolBpin] (M)	[*o*-TolBpin] (M)
1	1.86	–	0.138	–	–	–
2	–	1.84	–	0.0496	0.0687	0.00279
3	1.86	1.84	0.0946	0.01476	0.0225	0.000622
4[b]	1.86	1.84	0.0823	0.00922	0.0192	0

[a]Conditions: 13 mg catalyst, 0.070 M B_2Pin_2, 80 °C, stirring 1000 rpm, 280 min, after which the reaction is quantified by GC-FID (internal standard = hexadecane, 0.067 M). [b]2.61 mg $[Ir(COD)Cl]_2$ (0.0039 mmol), 1.4 mg 1,10-phenanthroline (0.0078 mmol), 0.070 M B_2Pin_2, 80 °C, stirring 1000 rpm, 280 min, after which the reaction is quantified by GC-FID (internal standard = hexadecane, 0.067 M).

https://dx.doi.org/10.1021/acs.organomet.9b00874
Organometallics XXXX, XXX, XXX−XXX

CONCLUSIONS

The immobilization of molecular iridium borylation catalysts into supports such as MOFs has led to improvements in chemoselectivity.[31,32,34−37,40,41] While a great deal of mechanistic work has occurred with homogeneous organoiridium borylation systems, the mechanistic implications of conducting borylation in the pores of a microporous material have not been fully explored experimentally. We have investigated the mechanistic aspects of a phenanthroline-ligated Ir catalyst immobilized in UiO-67 to gain insight into intrinsic features of this borylation reaction. Characterization of the precatalyst structure before and after oxidation revealed information regarding ligand environment, notably the presence of an Ir−Cl bond by X-ray PDF/DED analysis. Affinity of the iridium−metalated MOF catalyst for aryl substrates such as benzene was demonstrated via benzene vapor sorption. An induction period was revealed in time course profiles of benzene borylation, which was perturbed through variation in amount of arene that was present in the system, and mass transport effects were found to greatly effect reaction rate over time. Overall, a rate law zero-order in B_2Pin_2 and first-order in arene is consistent with the presented kinetic observations; however, this behavior may also be ascribed, in part, to activation of the catalyst. Monitoring borylation of benzene-d_6 revealed a primary kinetic isotope effect in the profile, while borylation of toluene demonstrated the competency of the catalyst to borylate alternative aryl substrates with slightly greater selectivity for benzene over toluene. Borylation of more sterically encumbered substrates such as *t*-butylbenzene was found to be challenging, which may indicate a size exclusion effect. Characterization of materials after catalysis also showed a deficiency of boron present, indicating a lack of accumulation which is a deviation from previously observed homogeneous behavior.

A preliminary understanding of the dynamics of this MOF-based borylation system and catalyst speciation has been established. Through efforts such as studying larger substrates than benzene and further experimentation regarding mitigation of the induction period and mass transport effects of this reaction, further experimental insight may be gained to establish a catalytic cycle for this process, in particular highlighting deviations from well-understood homogeneous systems.

ASSOCIATED CONTENT

Supporting Information

The Supporting Information is available free of charge at https://pubs.acs.org/doi/10.1021/acs.organomet.9b00874.

Experimental materials and methods, synthetic procedures, characterization of materials (PDF)

AUTHOR INFORMATION

Corresponding Authors

David M. Kaphan − *Chemical Sciences and Engineering Division, Argonne National Laboratory, Lemont, Illinois 60439, United States;* orcid.org/0000-0001-5293-7784; Email: kaphand@anl.gov

Massimiliano Delferro − *Chemical Sciences and Engineering Division, Argonne National Laboratory, Lemont, Illinois 60439, United States;* orcid.org/0000-0002-4443-165X; Email: delferro@anl.gov

Omar K. Farha − *Department of Chemistry and International Institute of Nanotechnology, Northwestern University, Evanston, Illinois 60208, United States;* orcid.org/0000-0002-9904-9845; Email: o-farha@u.northwestern.edu

Authors

Zoha H. Syed − *Department of Chemistry and International Institute of Nanotechnology, Northwestern University, Evanston, Illinois 60208, United States; Chemical Sciences and Engineering Division, Argonne National Laboratory, Lemont, Illinois 60439, United States;* orcid.org/0000-0002-0074-2253

Zhihengyu Chen − *Department of Chemistry, Stony Brook University, Stony Brook, New York 11764, United States*

Karam B. Idrees − *Department of Chemistry and International Institute of Nanotechnology, Northwestern University, Evanston, Illinois 60208, United States;* orcid.org/0000-0002-9603-3952

Timothy A. Goetjen − *Department of Chemistry and International Institute of Nanotechnology, Northwestern University, Evanston, Illinois 60208, United States;* orcid.org/0000-0001-8023-9107

Evan C. Wegener − *Chemical Sciences and Engineering Division, Argonne National Laboratory, Lemont, Illinois 60439, United States*

Xuan Zhang − *Department of Chemistry and International Institute of Nanotechnology, Northwestern University, Evanston, Illinois 60208, United States;* orcid.org/0000-0001-8214-7265

Karena W. Chapman − *Department of Chemistry, Stony Brook University, Stony Brook, New York 11764, United States;* orcid.org/0000-0002-8725-5633

Complete contact information is available at: https://pubs.acs.org/10.1021/acs.organomet.9b00874

Funding

This work was supported by the Inorganometallic Design Center, an Energy Frontier Research Center (EFRC) funded by the U.S. Department of Energy (DOE), Office of Science, Basic Energy Sciences (DE-SC0012702). This material is based upon work supported by the National Science Foundation Graduate Research Fellowship under Grant No. (DGE-1842165) (Z.H.S.). Use of the Advanced Photon Source (APS) at Argonne National Laboratory is funded by the U.S. DOE under contract DE-AC-02-06CH11357. MRCAT operations are supported by the U.S. DOE and the MRCAT member institutions. X-ray pair distribution function (PDF) and differential envelope density (DED) analyses were obtained at 11-ID-B at the APS at Argonne National Laboratory. This work made use of the IMSERC at Northwestern University, which has received support from the Soft and Hybrid Nanotechnology Experimental (SHyNE) Resource (NSF ECCS-1542205), the State of Illinois, and the International Institute for Nanotechnology (IIN). For NMR work on the Au400, this work made use of the IMSERC at Northwestern University, which has received support from the NSF (CHE-1048773); Soft and Hybrid Nanotechnology Experimental (SHyNE) Resources (NSF ECCS-1542205); the State of Illinois and International Institute for Nanotechnology (IIN). This work also made use of the Keck-II facility of Northwestern University's NUANCE Center, which has received support from the Soft and Hybrid Nanotechnology Experimental (SHyNE) Resource (NSF ECCS-

https://dx.doi.org/10.1021/acs.organomet.9b00874
Organometallics XXXX, XXX, XXX−XXX

1542205); the MRSEC program (NSF DMR-1720139) at the Materials Research Center; the International Institute for Nanotechnology (IIN); the Keck Foundation; and the State of Illinois, through the IIN. In addition, this work made use of the EPIC facility of Northwestern University's NUANCE Center, which has received support from the Soft and Hybrid Nanotechnology Experimental (SHyNE) Resource (NSF ECCS-1542205); the MRSEC program (NSF DMR-1720139) at the Materials Research Center; the International Institute for Nanotechnology (IIN); the Keck Foundation; and the State of Illinois, through the IIN. Metal analysis was performed at the Northwestern University Quantitative Bioelement Imaging Center. Molecular graphics and analyses were performed with UCSF Chimera, developed by the Resource for Biocomputing, Visualization, and Informatics at the University of California, San Francisco, with support from NIH P41-GM103311.

Notes

The authors declare no competing financial interest.

■ ACKNOWLEDGMENTS

The authors thank Dr. Magali S. Ferrandon for initial kinetics protocol optimization and GC method development, Dr. Xingjie Wang for initial XPS measurements, Ms. Rebecca Sponenburg for microwave digestion of MOF samples for ICP-OES analysis to quantify boron, and Dr. Timur Islamoglu and Dr. Zhijie Chen for helpful discussions.

■ REFERENCES

(1) Labinger, J. A.; Bercaw, J. E. Understanding and Exploiting C-H Bond Activation. *Nature* **2002**, *417*, 507−514.
(2) Hartwig, J. F. Evolution of C-H Bond Functionalization from Methane to Methodology. *J. Am. Chem. Soc.* **2016**, *138*, 2−24.
(3) Mkhalid, I. A. I.; Barnard, J. H.; Marder, T. B.; Murphy, J. M.; Hartwig, J. F. C-H Activation for the Construction of C-B Bonds. *Chem. Rev.* **2010**, *110* (2), 890−931.
(4) Hartwig, J. F. Borylation and Silylation of C-H Bonds: A Platform for Diverse C-H Bond Functionalizations. *Acc. Chem. Res.* **2012**, *45* (6), 864−873.
(5) Xu, L.; Wang, G.; Zhang, S.; Wang, H.; Wang, L.; Liu, L.; Jiao, J.; Li, P. Recent Advances in Catalytic C−H Borylation Reactions. *Tetrahedron* **2017**, *73*, 7123−7157.
(6) Iverson, C. N.; Smith, M. R. Stoichiometric and Catalytic B-C Bond Formation from Unactivated Hydrocarbons and Boranes [1]. *J. Am. Chem. Soc.* **1999**, *121*, 7696−7697.
(7) Cho, J. Y.; Iverson, C. N.; Smith, M. R. Steric and Chelate Directing Effects in Aromatic Borylation [3]. *J. Am. Chem. Soc.* **2000**, *122* (51), 12868−12869.
(8) Cho, J. Y.; Tse, M. K.; Holmes, D.; Maleczka, R. E.; Smith, M. R. Remarkably Selective Iridium Catalysts for the Elaboration of Aromatic C-H Bonds. *Science (Washington, DC, U. S.)* **2002**, *295* (5553), 305−308.
(9) Ishiyama, T.; Takagi, J.; Ishida, K.; Miyaura, N.; Anastasi, N. R.; Hartwig, J. F. Mild Iridium-Catalyzed Borylation of Arenes. High Turnover Numbers, Room Temperature Reactions, and Isolation of a Potential Intermediate. *J. Am. Chem. Soc.* **2002**, *124* (3), 390−391.
(10) Ishiyama, T.; Takagi, J.; Hartwig, J. F.; Miyaura, N. A Stoichiometric Aromatic C-H Borylation Catalyzed by Iridium(I)/2,2′-Bipyridine Complexes at Room Temperature. *Angew. Chem., Int. Ed.* **2002**, *41* (16), 3056−3058.
(11) Hartwig, J. F. Regioselectivity of the Borylation of Alkanes and Arenes. *Chem. Soc. Rev.* **2011**, *40*, 1992−2002.
(12) Larsen, M. A.; Hartwig, J. F. Iridium-Catalyzed C-H Borylation of Heteroarenes: Scope, Regioselectivity, Application to Late-Stage Functionalization, and Mechanism. *J. Am. Chem. Soc.* **2014**, *136* (11), 4287−4299.
(13) Larsen, M. A.; Wilson, C. V.; Hartwig, J. F. Iridium-Catalyzed Borylation of Primary Benzylic C-H Bonds without a Directing Group: Scope, Mechanism, and Origins of Selectivity. *J. Am. Chem. Soc.* **2015**, *137* (26), 8633−8643.
(14) Oeschger, R. J.; Larsen, M. A.; Bismuto, A.; Hartwig, J. F. Origin of the Difference in Reactivity between Ir Catalysts for the Borylation of C-H Bonds. *J. Am. Chem. Soc.* **2019**, *141* (41), 16479−16485.
(15) Takagi, J.; Sato, K.; Hartwig, J. F.; Ishiyama, T.; Miyaura, N. Iridium-Catalyzed C-H Coupling Reaction of Heteroaromatic Compounds with Bis(Pinacolato)Diboron: Regioselective Synthesis of Heteroarylboronates. *Tetrahedron Lett.* **2002**, *43* (32), 5649−5651.
(16) Ishiyama, T.; Nobuta, Y.; Hartwig, J. F.; Miyaura, N. Room Temperature Borylation of Arenes and Heteroarenes Using Stoichiometric Amounts of Pinacolborane Catalyzed by Iridium Complexes in an Inert SolventElectronic Supplementary Information (ESI) Available: Experimental Procedures and Spectral Analyses of P. *Chem. Commun.* **2003**, No. 23, 2924.
(17) Ishiyama, T.; Takagi, J.; Yonekawa, Y.; Hartwig, J. F.; Miyaura, N. Iridium-Catalyzed Direct Borylation of Five-Membered Heteroarenes by Bis(Pinacolato)Diboron: Regioselective, Stoichiometric, and Room Temperature Reactions. *Adv. Synth. Catal.* **2003**, *345* (910), 1103−1106.
(18) Boebel, T. A.; Hartwig, J. F. Silyl-Directed, Iridium-Catalyzed Ortho-Borylation of Arenes. A One-Pot Ortho-Borylation of Phenols, Arylamines, and Alkylarenes. *J. Am. Chem. Soc.* **2008**, *130* (24), 7534−7535.
(19) Boller, T. M.; Murphy, J. M.; Hapke, M.; Ishiyama, T.; Miyaura, N.; Hartwig, J. F. Mechanism of the Mild Functionalization of Arenes by Diboron Reagents Catalyzed by Iridium Complexes. Intermediacy and Chemistry of Bipyridine-Ligated Iridium Trisboryl Complexes. *J. Am. Chem. Soc.* **2005**, *127* (41), 14263−14278.
(20) Vanchura, B. A., II; Preshlock, S. M.; Roosen, P. C.; Kallepalli, V. A.; Staples, R. J.; Maleczka, R. E., Jr.; Singleton, D. A.; Smith, M. R., III Electronic Effects in Iridium C-H Borylations: Insights from Unencumbered Substrates and Variation of Boryl Ligand Substituents. *Chem. Commun.* **2010**, *46* (41), 7724−7726.
(21) Ji, L.; Fucke, K.; Bose, S. K.; Marder, T. B. Iridium-Catalyzed Borylation of Pyrene: Irreversibility and the Influence of Ligand on Selectivity. *J. Org. Chem.* **2015**, *80* (1), 661−665.
(22) Jover, J.; Maseras, F. Mechanistic Investigation of Iridium-Catalyzed C-H Borylation of Methyl Benzoate: Ligand Effects in Regioselectivity and Activity. *Organometallics* **2016**, *35* (18), 3221−3226.
(23) Chattopadhyay, B.; Dannatt, J. E.; Andujar-De Sanctis, I. L.; Gore, K. A.; Maleczka, R. E.; Singleton, D. A.; Smith, M. R. Ir-Catalyzed Ortho-Borylation of Phenols Directed by Substrate-Ligand Electrostatic Interactions: A Combined Experimental/in Silico Strategy for Optimizing Weak Interactions. *J. Am. Chem. Soc.* **2017**, *139* (23), 7864−7871.
(24) Montero Bastidas, J. R.; Oleskey, T. J.; Miller, S. L.; Smith, M. R.; Maleczka, R. E. Para-Selective, Iridium-Catalyzed C-H Borylations of Sulfated Phenols, Benzyl Alcohols, and Anilines Directed by Ion-Pair Electrostatic Interactions. *J. Am. Chem. Soc.* **2019**, *141* (39), 15483−15487.
(25) Zatsepin, P.; Sorsche, D.; Ahn, S.; Baik, M.-H.; Mindiola, D. J. Catalytic Borylation of Methane: Combining Computational and High-Throughput Screening Approaches to Discover a New Catalyst. *Alkane Functionalization* **2018**, 337−369.
(26) Cook, A. K.; Schimler, S. D.; Matzger, A. J.; Sanford, M. S. Catalyst-Controlled Selectivity in the C-H Borylation of Methane and Ethane. *Science (Washington, DC, U. S.)* **2016**, *351* (6280), 1421−1424.
(27) Smith, K. T.; Berritt, S.; González-Moreiras, M.; Ahn, S.; Smith, M. R.; Baik, M. H.; Mindiola, D. J. Catalytic Borylation of Methane. *Science (Washington, DC, U. S.)* **2016**, *351* (6280), 1424−1427.
(28) Preshlock, S. M.; Ghaffari, B.; Maligres, P. E.; Krska, S. W.; Maleczka, R. E.; Smith, M. R. High-Throughput Optimization of Ir-

https://dx.doi.org/10.1021/acs.organomet.9b00874
Organometallics XXXX, XXX, XXX−XXX

Catalyzed C-H Borylation: A Tutorial for Practical Applications. *J. Am. Chem. Soc.* **2013**, *135* (20), 7572−7582.
(29) Liskey, C. W.; Hartwig, J. F. Iridium-Catalyzed Borylation of Secondary C-H Bonds in Cyclic Ethers. *J. Am. Chem. Soc.* **2012**, *134* (30), 12422−12425.
(30) Coventry, D. N.; Batsanov, A. S.; Goeta, A. E.; Howard, J. A. K.; Marder, T. B.; Perutz, R. N. Selective Ir-Catalysed Borylation of Polycyclic Aromatic Hydrocarbons: Structures of Naphthalene-2,6-Bis(Boronate), Pyrene-2,7-Bis(Boronate) and Perylene-2,5,8,11-Tetra(Boronate) Esters. *Chem. Commun.* **2005**, No. 16, 2172−2174.
(31) Chen, Q.; Dong, A.; Wang, D.; Qiu, L.; Ma, C.; Yuan, Y.; Zhao, Y.; Jia, N.; Guo, Z.; Wang, N. Efficient and Selective Methane Borylation Through Pore Size Tuning of Hybrid Porous Organic-Polymer-Based Iridium Catalysts. *Angew. Chem., Int. Ed.* **2019**, *58* (31), 10671−10676.
(32) Tahir, N.; Muniz-Miranda, F.; Everaert, J.; Tack, P.; Heugebaert, T.; Leus, K.; Vincze, L.; Stevens, C. V.; Van Speybroeck, V.; Van Der Voort, P. Immobilization of Ir(I) Complex on Covalent Triazine Frameworks for C−H Borylation Reactions: A Combined Experimental and Computational Study. *J. Catal.* **2019**, *371*, 135−143.
(33) Copéret, C.; Comas-Vives, A.; Conley, M. P.; Estes, D. P.; Fedorov, A.; Mougel, V.; Nagae, H.; Núnez-Zarur, F.; Zhizhko, P. A. Surface Organometallic and Coordination Chemistry toward Single-Site Heterogeneous Catalysts: Strategies, Methods, Structures, and Activities. *Chem. Rev.* **2016**, *116*, 323−421.
(34) Feng, X.; Song, Y.; Li, Z.; Kaufmann, M.; Pi, Y.; Chen, J. S.; Xu, Z.; Li, Z.; Wang, C.; Lin, W. Metal-Organic Framework Stabilizes a Low-Coordinate Iridium Complex for Catalytic Methane Borylation. *J. Am. Chem. Soc.* **2019**, *141* (28), 11196−11203.
(35) Gonzalez, M. I.; Bloch, E. D.; Mason, J. A.; Teat, S. J.; Long, J. R. Single-Crystal-to-Single-Crystal Metalation of a Metal-Organic Framework: A Route toward Structurally Well-Defined Catalysts. *Inorg. Chem.* **2015**, *54* (6), 2995−3005.
(36) Mamlouk, H.; Suriboot, J.; Manyam, P. K.; Alyazidi, A.; Bergbreiter, D. E.; Madrahimov, S. T. Highly Active, Separable and Recyclable Bipyridine Iridium Catalysts for C-H Borylation Reactions. *Catal. Sci. Technol.* **2018**, *8* (1), 124−127.
(37) Manna, K.; Zhang, T.; Lin, W. Postsynthetic Metalation of Bipyridyl-Containing Metal-Organic Frameworks for Highly Efficient Catalytic Organic Transformations. *J. Am. Chem. Soc.* **2014**, *136* (18), 6566−6569.
(38) Kimura, A.; Hayama, H.; Hasegawa, J. Y.; Nageh, H.; Wang, Y.; Naga, N.; Nishida, M.; Nakano, T. Recyclable and Efficient Polyurethane-Ir Catalysts for Direct Borylation of Aromatic Compounds. *Polym. Chem.* **2017**, *8* (47), 7406−7415.
(39) Manna, K.; Zhang, T.; Greene, F. X.; Lin, W. Bipyridine- and Phenanthroline-Based Metal-Organic Frameworks for Highly Efficient and Tandem Catalytic Organic Transformations via Directed C-H Activation. *J. Am. Chem. Soc.* **2015**, *137* (7), 2665−2673.
(40) Zhang, X.; Huang, Z.; Ferrandon, M.; Yang, D.; Robison, L.; Li, P.; Wang, T. C.; Delferro, M.; Farha, O. K. Catalytic Chemoselective Functionalization of Methane in a Metal-Organic Framework. *Nat. Catal.* **2018**, *1* (5), 356−362.
(41) Dhakshinamoorthy, A.; Asiri, A. M.; Garcia, H. Formation of C-C and C-Heteroatom Bonds by C-H Activation by Metal Organic Frameworks as Catalysts or Supports. *ACS Catal.* **2019**, *9* (2), 1081−1102.
(42) Nguyen, P.; Blom, H. P.; Westcott, S. A.; Taylor, N. J.; Marder, T. B. Synthesis and Structures of the First Transition-Metal Tris(Boryl) Complexes: (H6-Arene)Ir(BO2C6H4)3. *J. Am. Chem. Soc.* **1993**, *115* (20), 9329−9330.
(43) Chotana, G. A.; Vanchura, B. A., II; Tse, M. K.; Staples, R. J.; Maleczka, R. E., Jr.; Smith, M. R., III Getting the Sterics Just Right: A Five-Coordinate Iridium Trisboryl Complex That Reacts with C-H Bonds at Room Temperature. *Chem. Commun.* **2009**, No. 38, 5731−5733.
(44) Zhu, L.; Qi, X.; Li, Y.; Duan, M.; Zou, L.; Bai, R.; Lan, Y. Ir(III)/Ir(V) or Ir(I)/Ir(III) Catalytic Cycle? Steric-Effect-Controlled Mechanism for the Para-C-H Borylation of Arenes. *Organometallics* **2017**, *36* (11), 2107−2115.
(45) Zhong, R. L.; Sakaki, S. Sp3 C-H Borylation Catalyzed by Iridium(III) Triboryl Complex: Comprehensive Theoretical Study of Reactivity, Regioselectivity, and Prediction of Excellent Ligand. *J. Am. Chem. Soc.* **2019**, *141* (25), 9854−9866.
(46) Tamura, H.; Yamazaki, H.; Sato, H.; Sakaki, S. Iridium-Catalyzed Borylation of Benzene with Diboron. Theoretical Elucidation of Catalytic Cycle Including Unusual Iridium(V) Intermediate. *J. Am. Chem. Soc.* **2003**, *125* (51), 16114−16126.
(47) Ahn, S.; Sorsche, D.; Berritt, S.; Gau, M. R.; Mindiola, D. J.; Baik, M. H. Rational Design of a Catalyst for the Selective Monoborylation of Methane. *ACS Catal.* **2018**, *8* (11), 10021−10031.
(48) Yang, B.; Wu, X. P.; Gagliardi, L.; Truhlar, D. G. Methane Functionalization by an Ir(III) Catalyst Supported on a Metal−Organic Framework: An Alternative Explanation of Steric Confinement Effects. *Theor. Chem. Acc.* **2019**, DOI: 10.1007/s00214-019-2498-y.
(49) Seechurn, C. C. C. J.; Sivakumar, V.; Satoskar, D.; Colacot, T. J. Iridium-Catalyzed C-H Borylation of Heterocycles Using an Overlooked 1,10-Phenanthroline Ligand: Reinventing the Catalytic Activity by Understanding the Solvent-Assisted Neutral to Cationic Switch. *Organometallics* **2014**, *33* (13), 3514−3522.
(50) Freakley, S. J.; Ruiz-Esquius, J.; Morgan, D. J. The X-Ray Photoelectron Spectra of Ir, IrO2 and IrCl3 Revisited. *Surf. Interface Anal.* **2017**, *49* (8), 794−799.
(51) Burés, J. Variable Time Normalization Analysis: General Graphical Elucidation of Reaction Orders from Concentration Profiles. *Angew. Chem., Int. Ed.* **2016**, *55* (52), 16084−16087.
(52) Blackmond, D. G. Reaction Progress Kinetic Analysis: A Powerful Methodology for Mechanistic Studies of Complex Catalytic Reactions. *Angew. Chem., Int. Ed.* **2005**, *44*, 4302−4320.
(53) Blackmond, D. G. Kinetic Profiling of Catalytic Organic Reactions as a Mechanistic Tool. *J. Am. Chem. Soc.* **2015**, *137*, 10852−10866.

https://dx.doi.org/10.1021/acs.organomet.9b00874
Organometallics XXXX, XXX, XXX−XXX